Four-Dimensional Wave Transformations By Space-Time Metasurfaces

Sajjad Taravati, *Senior Member, IEEE*, and George V. Eleftheriades, *Fellow, IEEE*

***Abstract*—Static metasurfaces have shown to be prominent compact structures for reciprocal and frequency-invariant transformation of electromagnetic waves in space. However, incorporating temporal variation to static metasurfaces enables dynamic apparatuses which are capable of four-dimensional tailoring of both the spatial and temporal characteristics of electromagnetic waves, leading to functionalities that are far beyond the capabilities of conventional static metasurfaces. This includes nonreciprocal full-duplex wave transmission, pure frequency conversion, parametric wave amplification, space-time (ST) decomposition, and space-time wave diffraction. This paper overviews our recent progress on analysis and functionalities of ST metasurfaces and slabs to break reciprocity. We study different operation regimes of ST metasurfaces such as scattering and diffraction at ST interfaces, ST sinusoidally-varying surfaces and slabs, as well as transmissive and reflective ST metasurfaces.**

***Index Terms*—Space-time, metasurfaces, nonreciprocity, wave engineering, refractive index, electromagnetic modulation.**

I. Introduction

Controlled transformation of electromagnetic fields has advanced drastically in recent years thanks to the advent and evolution of metamaterials and metasurfaces [1]–[4]. Static metamaterials and metasurfaces allowed for substantial progress in wave engineering applications [5]. Recently, there has been a growing interest on four-dimensional metasurfaces, where adding the temporal variation to static metasurfaces leads to functionalities that are far beyond the capabilities of conventional static metasurfaces. For instance, asymmetric wave transmission can be achieved by spatially asymmetric structures when multiple modes are involved at different ports. On the other hand, nonreciprocal wave transmission is a far more challenging task that requires an external field for breaking the time-invariance of the structure [6], unilateral-transistor-loaded cells [3], or nonlinear materials [7]. Among these nonreciprocity approaches, space-time (ST) modulation is of high interest thanks to its immense capability for affecting the spectrum of the electromagnetic waves while breaking the time reversal symmetry.

ST metasurfaces provide huge degrees of freedom for arbitrary alteration of the wavevector and temporal frequency of electromagnetic waves, leading to an advanced four-dimensional wave processing from acoustics and microwaves [6], [8]–[10], [10]–[16] to terahertz and optics [17]–[21]. They represent a class of compact *dynamic wave processors*, which have been recently proposed for extraordinary manipulation of electromagnetic waves. Such four-dimensional compact apparatuses are endowed with unique properties not readily seen in conventional static metamaterials and metasurfaces. ST metasurfaces may take advantage of ST modulation capabilities, including nonreciprocal frequency generation [12], [16], [22], [23], parametric wave amplification [9], [24]–[26], asymmetric dispersion [27]–[29], and energy accumulation [30]. Frequency generation and nonreciprocity are of particular interest in ST-modulated (STM) slabs [16], [21], [22], [27], [29], [31]–[33], which are endowed by asymmetric periodic electromagnetic transitions in their dispersion diagram [13], [27], [28], [31], [34]. In practice, the ST modulation is achieved through pumping external energy into the medium [6], [11], [12], [22], [27], [35].

Some of the recently proposed applications of STM metamaterials and metasurfaces include mixer-duplexer-antennas [36], unidirectional beam splitters [11], nonreciprocal filters [37], [38], signal coding metasurfaces [15], [39], ST metasurfaces for advanced wave engineering and extraordinary control over electromagnetic waves [6], [8], [12]–[14], [17], [19], [40]–[48], nonreciprocal platforms [27], [29], [31], [48]–[52], frequency converters [12], [16], [22], [23], time-modulated antennas [53], [54] spectral camouflage metasurfaces [55], antenna-mixer-amplifiers [56], and enhanced resolution imaging photonic crystals [57]. This diverse and significant capability of STM media is due to their unique interactions with the incident field [27], [47], [58]–[61].

This paper provides a review on the properties of ST metasurfaces, their analysis, and their potential applications in modern and future wireless communication systems, and wave-tailoring processors. We first present key properties of ST interfaces, including spatial interfaces, temporal interfaces, and ST interfaces. Then, we show that a nonreciprocal metasurface acts as a very thin ST slab, i.e., a moving metasurface. Next, analysis of general STM metasurfaces is outlined, including derivation of scattered electromagnetic fields, four-dimensional dispersion diagrams, boundary conditions, and spatiotemporal decomposition. Then, full-wave finite-difference time domain (FDTD) simulation of ST metasurfaces are presented. Finally, illustrative examples are provided to show peculiar and unique functionalities of ST metasurfaces.

II. Electromagnetic Waves in ST Structure

Figure 1 shows the Minkowski ST diagram and its Fourier transformed pair known as the dispersion diagram. The four-dimensional Minkowski ST diagram includes two light cones,

Sajjad Taravati and George V. Eleftheriades are with the Edward S. Rogers Sr. Department of Electrical and Computer Engineering, University of Toronto, Toronto, Ontario M5S 3H7, Canada Email: sajjad.taravati@utoronto.ca.

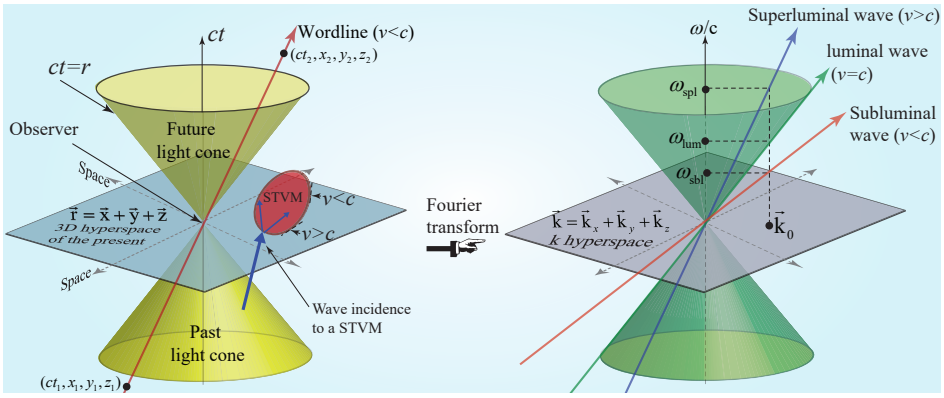

Fig. 1. ST Fourier pair diagrams.

representing propagation of the light in the past and future. The two cones have their apexes at the present, where the three-dimensional (x, y and z) hyperspace exists. Any discontinuity in the four dimensional ST diagram may result in forward and backward waves in space. Analysis and design of ST media and metasurfaces can be substantially eased by understanding the Fourier pair of the Minkowski diagram. To best investigate the wave diffraction by a STM grating, we first study the interaction of the electromagnetic wave with space and time interfaces, separately. In general, three different ST discontinuities may be studied as follows.

A. Space Interface

Figure 2(a) sketches the ST diagram of a spatial interface between two media of refractive indices n_1 and n_2, respectively, in the plane (z, ct). This figure shows scattering of forward and backward fields and conservation of energy and momentum for different scenarios. The temporal axis of the Minkowski ST diagram is scaled with the speed of light c, and therefore is labeled by ct for changing the dimension of the addressed physical quantity from time to length, in accordance to the dimension associated to the spatial axes labeled z. This problem represents the textbook case of electromagnetic wave incidence and scattering from a spatial (static) interface, where $n(z<0)=n_1$ and $n(z>0)=n_2$. The boundary conditions are derived by applying the fundamental physical fact that all physical quantities must remain bounded everywhere and at every time to the space and time derivatives in sourceless Maxwell equations

$$\nabla \times \mathbf{E} = -\frac{\partial \mathbf{B}}{\partial t} \quad \text{and} \quad \nabla \times \mathbf{H} = \frac{\partial \mathbf{D}}{\partial t}. \tag{1}$$

The discontinuity of the tangential components of electric and magnetic fields at $z = z_0$ would result in unbounded and singular electromagnetic fields at the interface, which is not physical. Therefore, the tangential components of the electric and magnetic fields must be continuous at a space discontinuity, i.e.,

$$\hat{z} \times (\mathbf{E}_2 - \mathbf{E}_1)|_{z=z_0} = 0 \quad \text{and} \quad \hat{z} \times (\mathbf{H}_2 - \mathbf{H}_1)|_{z=z_0} = 0. \tag{2}$$

As a result, the wavenumber k changes, i.e., energy is preserved but momentum changes, such that the forward transmitted wave in region 2 corresponds to $k_\mathrm{t} = k_\mathrm{i} n_2/n_1$, whereas the temporal frequency of the transmitted wave in region 2 is equal to that of region 1, i.e., $\omega_\mathrm{t} = \omega_\mathrm{i}$.

$$E_1 = \left(e^{ik_\mathrm{i}z} + Re^{-ik_\mathrm{i}z}\right) e^{-i\omega_\mathrm{i}t}, \quad \text{and} \quad E_2 = Te^{ik_\mathrm{t}z} e^{-i\omega_\mathrm{i}t}, \tag{3a}$$

where R and T represent the spatial reflection and transmission coefficients, and defined as

$$R = \frac{n_1 - n_2}{n_1 + n_2}, \quad \text{and} \quad T = \frac{2n_2}{n_1 + n_2}. \tag{3b}$$

B. Time Interface

Figure 2(b) shows the ST diagram of a time interface between two media of refractive indices n_1 and n_2, which is the dual case of the spatial metasurface in Fig. 2(a) [40], [62]. Here, the refractive index suddenly changes from one value (n_1) to another (n_2) at a given time throughout all space, i.e., $n(t<0)=n_1$ and $n(t>0)=n_2$. The temporal change of the refractive index produces both reflected (backward) and transmitted (forward) waves, which is analogous to the reflected and transmitted waves produced at the spatial interface between two different media in Fig. 2(a). The discontinuity of $\mathbf{D}$ and $\mathbf{B}$ at $ct = ct_0$ would result in unbounded and singular $\mathbf{E}$ and $\mathbf{H}$ at the interface, which is not physical. Therefore, $\mathbf{D}$ and $\mathbf{B}$ must be continuous at a time interface, that is,

$$(\mathbf{D}_2 - \mathbf{D}_1)|_{ct=ct_0} = 0 \quad \text{and} \quad (\mathbf{B}_2 - \mathbf{B}_1)|_{ct=ct_0} = 0. \tag{4}$$

The total charge Q and the total flux ψ must remain constant at the moment of the jump from n_1 to n_2, implying that both transversal and normal components of $\mathbf{D}$ and $\mathbf{B}$ do not change instantaneously [63], [64], which is different than the static case (shown in Fig. 2(a)) where only the normal components of the magnetic field $\mathbf{B}$ and electric field displacement $\mathbf{D}$ are conserved. Specifically, at a time interface, the magnetic field $\mathbf{B}$, the electric field displacement $\mathbf{D}$ and the wavenumber k are preserved. This yields a change in the temporal frequency of the incident wave so that the frequency of the forward transmitted wave in region 2 corresponds to $\omega_\mathrm{t} = \omega_\mathrm{i} n_1/n_2$, i.e., where momentum is preserved but energy changes.

$$D_1 = e^{ik_\mathrm{i}z} e^{-i\omega_\mathrm{i}t} \quad \text{and} \quad D_2 = e^{ik_\mathrm{i}z} \left(\widehat{T}e^{-i\omega_\mathrm{t}t} + \widehat{R}e^{i\omega_\mathrm{t}t}\right), \tag{5a}$$

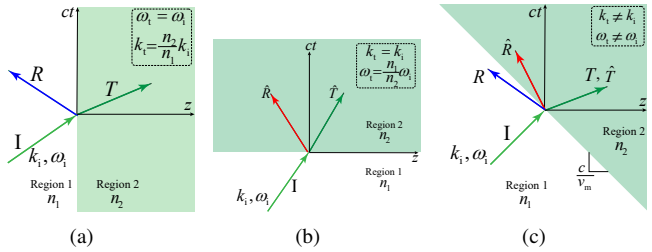

Fig. 2. ST diagrams showing scattering of forward and backward fields and conservation of energy and momentum for different scenarios. (a) Spatial interface, i.e., $n(z<0)=n_1$ and $n(z>0)=n_2$. (b) Temporal interface, i.e., $n(t<0)=n_1$ and $n(t>0)=n_2$. (c) ST interface, i.e., $n(z/c+t<0)=n_1$ and $n(z/c+t>0)=n_2$.

where $\widehat{R}$ and $\widehat{T}$ represent the temporal reflection and transmission coefficients, and defined as

$$\widehat{R}=\frac{n_1}{n_2}\frac{\eta_1-\eta_2}{2\eta_1}, \quad \text{and} \quad \widehat{T}=\frac{n_1}{n_2}\frac{\eta_1+\eta_2}{2\eta_1}. \tag{5b}$$

where $\eta_1=\sqrt{\mu_1/\epsilon_1}$ and $\eta_2=\sqrt{\mu_2/\epsilon_2}$.

C. Space-Time Interface

Figure 2(c) depicts the ST diagram of a ST interface, i.e., $n(z/c+t<0)=n_1$ and $n(z/c+t>0)=n_2$, as the combination of the space and time interfaces in Figs. 2(a) and 2(b), respectively. It may be seen that the ST interface resembles the spatial interface configuration in Fig. 2(a) in the region $n=n_1$ and the temporal interface configuration in Fig. 2(b) for $n=n_2$.

The reflection and transmission at a subluminal ST interface reads

$$R=\frac{\eta_2-\eta_1}{\eta_1+\eta_2}\frac{v_1-v_\mathrm{m}}{v_1+v_\mathrm{m}} \quad \text{and} \quad T=\frac{2\eta_2}{\eta_1+\eta_2}\frac{v_1-v_\mathrm{m}}{v_2-v_\mathrm{m}}, \tag{6a}$$

and the temporal and spatial frequencies of the reflected and transmitted waves read

$$\omega_R=\omega_\mathrm{i}\frac{v_1-v_\mathrm{m}}{v_1+v_\mathrm{m}}, \quad \text{and} \quad \omega_T=\omega_\mathrm{i}\frac{v_1-v_\mathrm{m}}{v_2-v_\mathrm{m}}, \tag{6b}$$

$$k_R=k_\mathrm{i}\frac{v_1-v_\mathrm{m}}{v_1+v_\mathrm{m}}, \quad \text{and} \quad k_T=k_\mathrm{i}\frac{v_1-v_\mathrm{m}}{v_2-v_\mathrm{m}}, \tag{6c}$$

where $v_1=c/n_1$ and $v_2=c/n_2$.

The reflection and transmission at a superluminal ST interface read

$$\widehat{R}=\frac{\eta_2-\eta_1}{2\eta_1}\frac{v_\mathrm{m}-v_1}{v_\mathrm{m}+v_2}, \quad \text{and} \quad \widehat{T}=\frac{\eta_1+\eta_2}{2\eta_1}\frac{v_\mathrm{m}-v_1}{v_\mathrm{m}-v_2}, \tag{7a}$$

and the temporal and spatial frequencies of the reflected and transmitted waves read

$$\omega_{\widehat{R}}=\omega_\mathrm{i}\frac{v_\mathrm{m}-v_1}{v_\mathrm{m}+v_2}, \quad \text{and} \quad \omega_{\widehat{T}}=\omega_\mathrm{i}\frac{v_\mathrm{m}-v_1}{v_\mathrm{m}-v_2}, \tag{7b}$$

$$k_{\widehat{R}}=k_\mathrm{i}\frac{v_\mathrm{m}-v_1}{v_\mathrm{m}+v_2}, \quad \text{and} \quad k_{\widehat{T}}=k_\mathrm{i}\frac{v_\mathrm{m}-v_1}{v_\mathrm{m}-v_2}. \tag{7c}$$

The pure-space interface is the $v_\mathrm{m}=0$ limit of a subluminal interface, while the pure-time interface is the $v_\mathrm{m}=\infty$ limit of a superluminal interface.

The difference between the excitation and response for validation of the symmetry and reciprocity of electromagnetic systems, associated with new frequency generation, is clarified in Figs. 3(a) and 3(b). Figure 3(a) shows the forward and backward problems for the symmetry test of a particular symmetric electromagnetic system, where the backward problem is represented by the spatial inversion of the forward problem, i.e., the applied excitation wave (input) of the backward problem must be the spatial inversion of the excitation wave (input) of the forward problem. As a result, for a symmetric system, the output of the backward problem would be exactly the spatial inversion of the output of the forward problem. Otherwise, the system is asymmetric. Figure 3(b) shows the forward and backward problems for the reciprocity test of a particular reciprocal electromagnetic system, where the backward problem is the spatial inversion of the *time-reversed* forward problem, i.e., the applied excitation wave (input) of the backward problem must be the spatial inversion of the output of the forward problem. As a result, for a reciprocal system, the output of the backward problem would be exactly the spatial inversion of the input of the forward problem. Otherwise, the system is nonreciprocal.

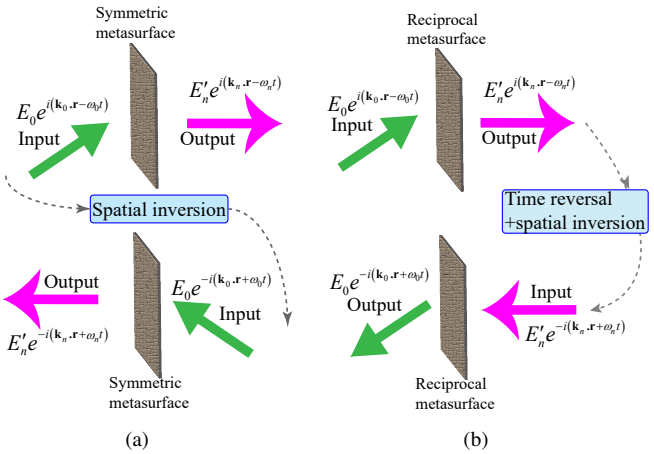

Fig. 3. Schematic of the experimental set-up configurations for validation of symmetric and reciprocal response of electromagnetic systems. (a) The electromagnetic symmetry of the system is validated, in which the backward problem is the *spatial inversion* of the forward problem. (b) The electromagnetic reciprocity of the system is validated, in which the backward problem is the *spatial inversion of the time-reversed* forward problem.

III. Experimental Demonstration of ST Interface

Transistor-loaded metasurfaces can represent a ST interface [2], [3], [9]. Figures 4(a) and 4(b) depict the operation principle of the nonreciprocal nongyrotropic metasurface. For $t<0$, the metasurface operates as a reflector where a $+z$-direction traveling wave is reflected by the metasurface and travels back along the $-z$ direction. For $t>0$, the metasurface operates as a nonreciprocal sheet, where a $+z$-direction traveling wave passes through the metasurface with gain and without polarization alteration, whereas a wave traveling along the opposite direction is being reflected by the metasurface. The transmission scattering parameters of the metasurface are not equal, i.e., $S_{21}>S_{12}$, where $S_{21}=\psi^\mathrm{F}_\mathrm{out}/\psi^\mathrm{F}_\mathrm{in}>1$ and $S_{12}=\psi^\mathrm{B}_\mathrm{out}/\psi^\mathrm{B}_\mathrm{in}<1$.

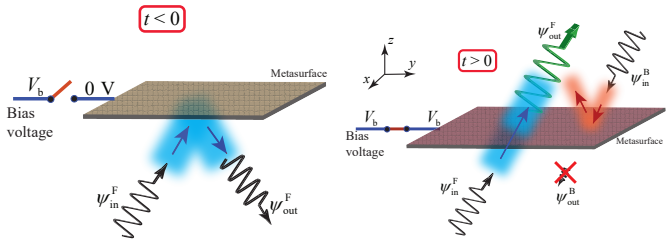

Fig. 4. Nonreciprocal nongyrotropic metasurface. (a) For $t > 0$ operating as a reflective sheet. (b) For $t > 0$ operating as a nonreciprocal transmissive sheet.

Figure 5(a) shows the full-wave simulation results, where transmission of waves from left to right is allowed and accompanied by power amplification but the transmission of waves from right to left is prohibited. Figure 5(b) shows an image of the fabricated metasurface [9]. The metasurface is formed by an array of unit cells. Such unit-cells are constituted of two microstrip patch elements interconnected through a unilateral transistor, introducing transmission gain in one direction and transmission loss in the other direction. Fig. 5(c) shows the measured transmission levels for both directions, and for $t < 0$ and $t > 0$. The nonreciprocal nongyrotropic metasurface in Fig. 5 may be represented as a moving metasurface in Fig. 6. The general case of a bianisotropic medium reads [9].

$$\boldsymbol{D} = \overline{\overline{\epsilon}} \cdot \boldsymbol{E} + \overline{\overline{\xi}} \cdot \boldsymbol{H}, \tag{8a}$$

$$\boldsymbol{B} = \overline{\overline{\zeta}} \cdot \boldsymbol{E} + \overline{\overline{\mu}} \cdot \boldsymbol{H}. \tag{8b}$$

The continuity equations of a metasurface may be expressed as

$$\hat{z} \times \Delta \boldsymbol{H} = j\omega\epsilon_0 \overline{\overline{\chi}}_{\text{ee}} \cdot \boldsymbol{E}_{\text{av}} + jk_0 \overline{\overline{\chi}}_{\text{em}} \cdot \boldsymbol{H}_{\text{av}}, \tag{9a}$$

$$\Delta \boldsymbol{E} \times \hat{z} = j\omega\mu_0 \overline{\overline{\chi}}_{\text{mm}} \cdot \boldsymbol{H}_{\text{av}} + jk_0 \overline{\overline{\chi}}_{\text{me}} \cdot \boldsymbol{E}_{\text{av}}, \tag{9b}$$

where Δ and the subscript 'av' represent, respectively, the difference of the fields and the average of the fields between the two sides of the metasurface. Eq. (9) provides a relation between the electromagnetic fields on the two sides of a metasurface and its susceptibilities, in the absence of normal susceptibility components. The constitutive parameters of the metasurface may be represented according to the susceptibilities in (9) as $\overline{\overline{\epsilon}} = \epsilon_0(\overline{\overline{I}} + \overline{\overline{\chi}}_{\text{ee}})$, $\overline{\overline{\mu}} = \mu_0(\overline{\overline{I}} + \overline{\overline{\chi}}_{\text{mm}})$, $\overline{\overline{\xi}} = \overline{\overline{\chi}}_{\text{em}}/c_0$, $\overline{\overline{\zeta}} = \overline{\overline{\chi}}_{\text{me}}/c_0$.

We then seek for the susceptibilities that provide the nonreciprocal nongyrotropic response of the metasurface by substituting the electromagnetic fields of the corresponding transformation into (9). Such a transformation includes passing a $+z$-propagating plane wave through the metasurface and complete absorption of a $-z$-propagating plane incident wave, yielding

$$\overline{\overline{\chi}}_{\text{ee}} = -\frac{j}{k_0}\begin{pmatrix} 1 & 0 \\ 0 & 1 \end{pmatrix}, \quad \overline{\overline{\chi}}_{\text{mm}} = -\frac{j}{k_0}\begin{pmatrix} 1 & 0 \\ 0 & 1 \end{pmatrix}, \tag{10a}$$

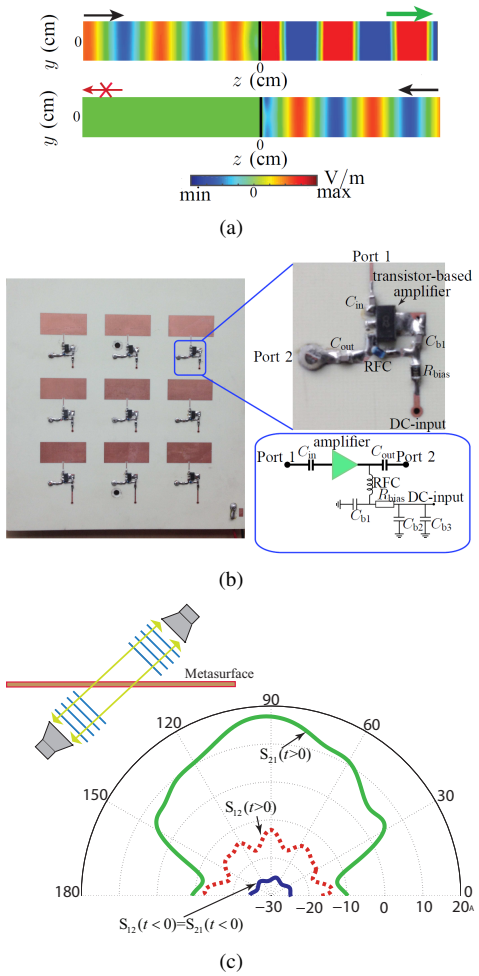

Fig. 5. Nonreciprocal metasurface. (a) Full-wave (FDTD) electric field distribution for excitations from the left and right (bottom) [9]. (b) An image of the fabricated metasurface [9]. (c) Experimental scattering parameters versus angle at $f = 5.9$ GHz for transmission in a straight line under an oblique angle [9].

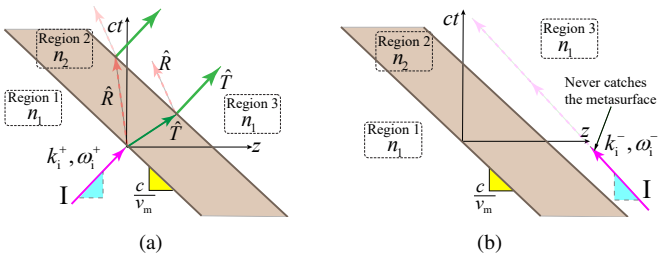

Fig. 6. ST representation of the nonreciprocal nongyrotropic metasurface in Figs. 4 and 5. (left) Forward wave incidence leading to full transmission, and (right) Backward wave incidence, where the wave can not catch up the metasurface.

$$\overline{\overline{\chi}}_{\text{em}} = \frac{j}{k_0}\begin{pmatrix} 0 & 1 \\ -1 & 0 \end{pmatrix}, \quad \overline{\overline{\chi}}_{\text{me}} = \frac{j}{k_0}\begin{pmatrix} 0 & -1 \\ 1 & 0 \end{pmatrix}, \tag{10b}$$

This shows that elements $\overline{\overline{\chi}}_{\text{em}}$ and $\overline{\overline{\chi}}_{\text{me}}$ are the ones that contribute to the nonreciprocity of the metasurface. The form of the susceptibility tensors in (10) is identical to that of a moving uniaxial medium.

IV. Analysis of ST Metasurface

Consider the STM structure in Fig. 7 characterized with the wavenumber $k_{\rm M}$ and possessing electric permittivity $\epsilon(z,t)$ and magnetic permeability $\mu(z,t)$, sandwiched between two semi-infinite unmodulated media, that is, region 1 characterized with the wavenumber $k_0 = \omega_0\sqrt{\epsilon_{\rm r,1}\mu_{\rm r,1}}/c = \sqrt{k_x^2+k_z^2}$ and region 3 with the wavenumber $k_0'' = \omega_0\sqrt{\epsilon_{\rm r,3}\mu_{\rm r,3}}/c = \sqrt{k_x''^2+k_z''^2}$. Here, ω_0 is the temporal frequency of the incident wave, $\epsilon_{\rm r,1}$ and $\epsilon_{\rm r,3}$ are electrical permitivitties of regions 1 and 3, respectively, and $\mu_{\rm r,1}$ and $\mu_{\rm r,3}$ are magnetic permeability of regions 1 and 3, respectively.

A general analysis assumes a metasurface with *temporally-periodic* electric permittivity and magnetic permeability, and a general *aperiodic/periodic* spatial variation [13]. Since the metasurface is time-periodic, its constitutive parameters may be expressed by a time-Floquet series expansion, as

$$\epsilon(z,t) = \sum_{s=-\infty}^{\infty} \epsilon_{k,\rm aper}(z) e^{is\Omega t}, \tag{11a}$$

$$\mu(z,t) = \sum_{s=-\infty}^{\infty} \mu_{k,\rm aper}(z) e^{is\Omega t}, \tag{11b}$$

where Ω is the temporal frequency of the modulation, and $\epsilon_{k,\rm aper}(z)$ and $\mu_{k,\rm aper}(z)$ are spatially-variant unknown coefficients of the permittivity and permeability, to be determined based on the spatial variation of the metasurface. We consider oblique incidence of a y-polarized electric field under angle of incidence of $\theta_{\rm I}$ to the metasurface, as

$$\mathbf{E}_{\rm I}(x,z,t) = \hat{\mathbf{y}} E_0 e^{i(k_x x + k_z z - \omega_0 t)}, \tag{12}$$

where E_0 is the amplitude of the incident wave. Given the temporal periodicity of the metasurface, the electric field inside the metasurface may be represented based on the temporal Bloch-Floquet decomposition as

$$\mathbf{E}_{\rm M}(x,z,t) = \hat{\mathbf{y}} \sum_{n,p} \mathbf{E}_{np} \left(A_{0p} e^{i\beta_{np}^{+} z} + B_{0p} e^{-i\beta_{np}^{-} z} \right) e^{i(k_x x - \omega_n t)}, \tag{13}$$

where $\omega_n = \omega_0 + n\Omega$. The scattered fields in regions 1 and 3 are

$$\mathbf{E}_{\rm R} = \hat{\mathbf{y}} \sum_{n,p} \left[E_{np} \left(A_{0p} + B_{0p} \right) - E_0 \delta_{n0} \right] e^{i[k_x x - k_{zn} z - \omega_n t]}, \tag{14a}$$

$$\mathbf{E}_{\rm T} = \hat{\mathbf{y}} \sum_{n,p} E_{np} \left(A_{0p} e^{i\beta_{np} L} + B_{0p} e^{-i\beta_{np} L} \right) e^{i\left[k_x'' x - k_{zn}'' z - \omega_n t\right]}. \tag{14b}$$

A. ST Decomposition

Figure 7 illustrates ST decomposition of space-time harmonics (STHs) in a spatiotemporally modulated structure. The scattering angles of the different space-time harmonics (STHs) may be determined from the Helmholtz relations where $k^2\sin^2(\theta_{\rm I}) + k_n^2\cos^2(\theta_{{\rm R}n}) = k_n^2$ and $k''^2\sin^2(\theta_{\rm I}) + k_n''^2\cos^2(\theta_{{\rm T}n}) = k_n''^2$, where $\theta_{{\rm R}n}$ and $\theta_{{\rm T}n}$ are the reflection and transmission angles of the $n^{\rm th}$ STH, yielding

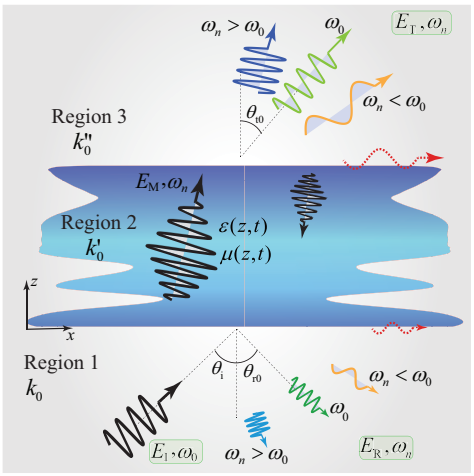

Fig. 7. ST decomposition resulting from oblique incidence to a STM metasurface [13].

$$\theta_{rn} = \theta_{{\rm t},n} = \sin^{-1}\left(\frac{\sin(\theta_{\rm I})}{1 + n\Omega/\omega_0} \right), \tag{15}$$

which demonstrates spectral decomposition of the scattered STHs. Considering $k' = k'' = k_0$, the reflection and transmission angles of the nth harmonic are equal, for equal tangential wavenumber, $k_x = k_0\sin(\theta_{\rm I})$ in all the regions. Eq. (15) shows that the harmonics in the n-interval $[\omega_0(\sin(\theta_{\rm I})-1)/\Omega, +\infty]$ are scattered (reflected and transmitted) at angles ranging from 0 to $\pi/2$ through $\theta_{\rm I}$ for $n=0$, while the STHs outside of this interval represent imaginary $k_{znp}'^{\pm}$ which do not scatter but rather propagate as surface waves along the boundary of the metasurface. The scattering angle of the pth mode of the nth STH inside the modulated medium reads

$$\theta_{np}^{\pm} = \tan^{-1}\left(\frac{k_x'}{k_{znp}'} \right) = \tan^{-1}\left(\frac{k_0'\sin(\theta_{\rm I})}{\beta_{0p}^{\pm} \pm nq} \right). \tag{16}$$

We consider a sinusoidally ST metasurface, as

$$\epsilon(z,t) = \epsilon_0\epsilon_{\rm r}\left[1 + \delta_\epsilon \sin(qz - \Omega t)\right], \tag{17a}$$

$$\mu(z,t) = \mu_0\mu_{\rm r}\left[1 + \delta_\mu \sin(qz - \Omega t)\right], \tag{17b}$$

where δ_ϵ and δ_μ represent respectively the permittivity and permeability modulation strengths. Such a metasurface is characterized with a ST-varying intrinsic impedance [29], i.e.,

$$\eta(z,t) = \sqrt{\frac{\mu_0\mu_{\rm r}\left[1 + \delta_\mu \sin(qz - \Omega t)\right]}{\epsilon_0\epsilon_{\rm r}\left[1 + \delta_\epsilon \sin(qz - \Omega t)\right]}}\Bigg|_{\delta_\mu = \delta_\epsilon} = \eta_0\eta_{\rm r} \tag{18}$$

Equation (18) reveals that such a STM metasurface exhibits zero space- and time local reflections as the intrinsic impedance of the metasurface is ST-independent.

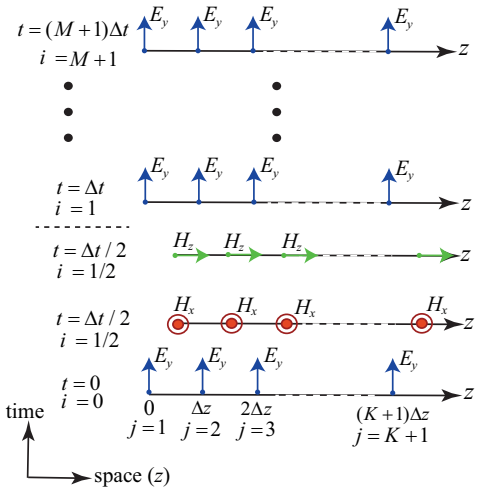

Fig. 8. General representation of the finite-difference time-domain scheme for numerical simulation of the oblique incidence of an E_y wave to STM slab [11].

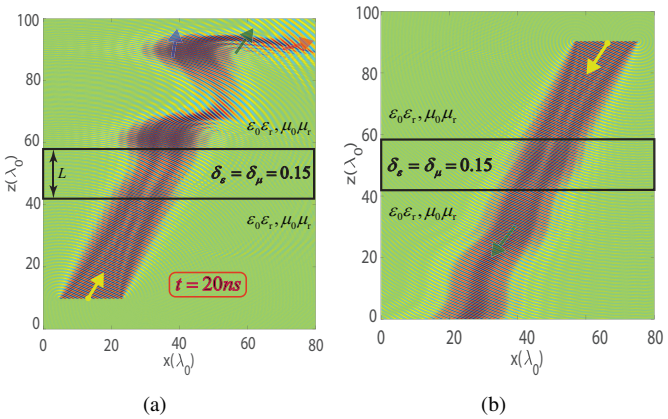

Fig. 9. Oblique excitation of the equilibrated STM metasurface, with a plane wave of frequency $\omega_0 = 2\pi \times 3$ GHz, with $\delta_\mu = \delta_\epsilon = 0.15$ and for $\theta_\mathrm{I} = 25°$. Numerical simulation result for the electric field distribution, E_y, at $t = 20$ ns [13]. (a) Forward transmission. (b) Backward transmission.

B. Numerical Simulation Scheme

To best gain insight into the wave propagation in ST metasurfaces and support the analytical solution we study the dynamic process through solving Maxwell's equations using FDTD numerical simulation. Figure 8 plots the implemented finite-difference time-domain scheme for numerical simulation of the oblique wave impinging on the STM slab. We first discretize the medium to $K+1$ spatial samples and $M+1$ temporal samples, with the steps of Δz and Δt, respectively. The finite-difference discretized form of the first two Maxwell's equations for the electric and magnetic fields are simplified to

$$H_x|_{j+1/2}^{i+1/2} = (1-\Delta t)\, H_x|_{j+1/2}^{i-1/2} + \frac{\Delta t}{\mu_0 \Delta z}\left(E_y|_{j+1}^{i} - E_y|_{j}^{i}\right) \tag{19a}$$

$$H_z|_{j+1/2}^{i+1/2} = (1-\Delta t)\, H_z|_{j+1/2}^{i-1/2} - \frac{\Delta t}{\mu_0 \Delta z}\left(E_y|_{j+1}^{i} - E_y|_{j}^{i}\right) \tag{19b}$$

$$E_y|_{j}^{i+1} = \left(1 - \frac{\Delta t \epsilon'|_j^i}{\epsilon|_j^{i+1/2}}\right) E_y|_j^i + \frac{\Delta t/\Delta z}{\epsilon|_j^{i+1/2}} \cdot \left[\left(H_x|_{j+1/2}^{i+1/2} - H_x|_{j-1/2}^{i+1/2}\right) - \left(H_z|_{j+1/2}^{i+1/2} - H_z|_{j-1/2}^{i+1/2}\right)\right] \tag{19c}$$

where $\epsilon' = \partial\epsilon(z,t)/\partial t = -\Omega\delta_\epsilon \cos(qz - \Omega t)$.

C. Wave Engineering Based on Unidirectional Frequency Generation and ST Decomposition

This section investigates the wave transmission and reflection from STM media using the FDTD numerical simulation. We consider oblique incidence to general STM metasurfaces, and compare the numerical results with the analytical solution provided in Sec. IV. A plane wave with temporal frequency $\omega_0 = 2\pi \times 3$ GHz is propagating along the $+z$-direction under an angle of incidence of $\theta_\mathrm{I} = 25°$, and impinges on the ST permittivity-modulated metasurface with the constitutive parameters in (17), where $\Omega = 2\pi \times 0.1$ GHz, $\Gamma = 1$, $L = 16\lambda_0$.

Next, we investigate the field scattering from an equilibrated STM metasurface, i.e. $\delta_\mu = \delta_\epsilon = 0.15$. Figures 9(a) and 9(b) plot the electric field distribution inside the modulated region and scattering outside the metasurface at $t = 20$ ns for forward and backward wave incidences, respectively. It may be seen from these two figures that, an equilibrated STM metasurface with $\delta_\mu = \delta_\epsilon = 0.15$ exhibits strong frequency generation, ST decomposition, and nonreciprocal wave transmission. It may be shown that an equilibrated STM metasurface with $\delta_\mu = \delta_\epsilon = 0.15$ may be realized with the same amount of pumping energy required for the realization of conventional permittivity-modulated metasurface with $\delta_\epsilon = 0.15$ and $\delta_\mu = 0$ [29]. Moreover, as we see in Fig. 9(a), the equilibrated metasurface exhibits zero local space and time reflection. The strict zero reflection from such a metasurface can be shown by increasing the number of space and time samples in the numerical scheme.

V. Diffraction Regime of ST Metasurfaces

The analysis provided in the previous section is applicable for ST metasurfaces operating outside the diffraction regime. This section analyses ST metasurfaces that provide spatial diffractions, where each spatial diffraction order (denoted by m) is comprising an infinite number of temporal diffraction orders(denoted by n). Figure 10(a) shows a generic illustration example of a wavevector isofrequency diagram for the diffraction from a STP diffraction grating. The grating is characterized with the spatial frequency K (the spatial periodicity of the STP grating reads $\Lambda = 2\pi/K$) and the temporal frequency Ω. Figure 10(a) sketches the phase matching of ST harmonic components of the total field inside the grating with propagating backward diffracted orders in region 1, and forward diffracted orders in region 3. We assume the grating is interfaced with two semifinite dielectrics, i.e., $z \to -\infty <$ region $1 < z = 0$ and $d <$ region $3 < z \to \infty$, respectively. Region 1, region 2 (inside the STP grating) and region

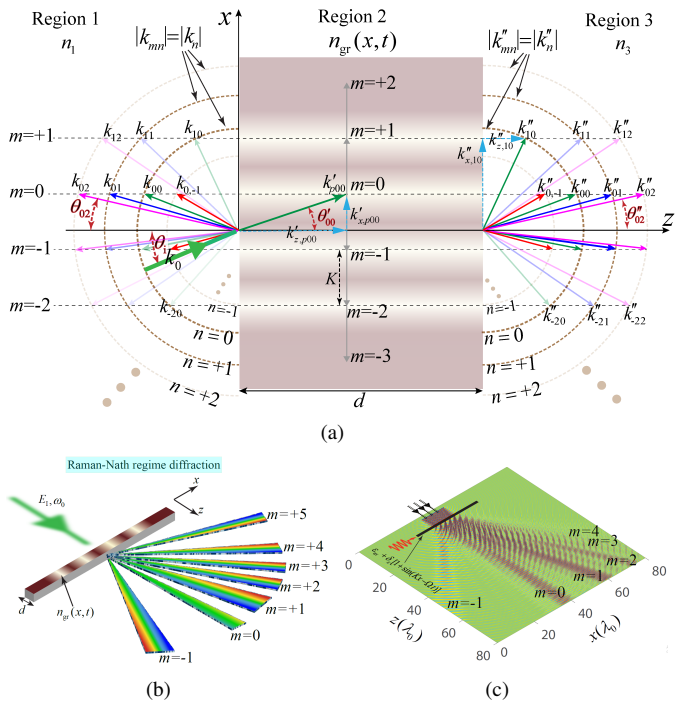

Fig. 10. Diffraction from a transmissive grating for a monochromatic incident wave. (a) Wavevector isofrequency diagram for the diffraction from a STP diffraction grating [15]. (b) and (c) Raman-Nath regime diffraction of a thin grating, where $\Omega = 0.4\omega_0$ and $K = 0.4k_0$, $\delta_\epsilon = 0.5$ and $d = 0.5\lambda$ [15].

3 are, respectively, characterized with the phase velocities $v_\mathrm{r} = c/n_1$, $v'_\mathrm{r} = c/n_\mathrm{av}$ and $v''_\mathrm{r} = c/n_3$, and the wavevectors $\mathbf{k}_{mn} = k_{x,mn}\hat{\mathbf{x}} + k_{z,mn}\hat{\mathbf{z}}$, $\mathbf{k}'_{pmn} = k'_{x,pmn}\hat{\mathbf{x}} + k'_{z,pmn}\hat{\mathbf{z}}$, and $\mathbf{k}''_{mn} = k''_{x,mn}\hat{\mathbf{x}} + k''_{z,mn}\hat{\mathbf{z}}$. Here, c represents the velocity of the light in vacuum, m and n denote the number of the space and time harmonics, respectively, while p represents the number of the mode in region 2, inside the grating (these modes only exist inside the grating).

Figures 10(b) and 10(c) show a generic representation of the ST diffraction from a STP diffraction grating, which is distinctly different from the spatial diffraction from a conventional space-periodic diffraction grating. The grating is interfaced with two semi-infinite dielectric regions, i.e., region 1 is characterized with the refractive index n_1 and wavenumber k, and region 3 is characterized with the refractive index n_3 and wavenumber k''. The relative electric permittivity of this STP grating is periodic in both space and time, with temporal frequency Ω and spatial frequency K, given by $n^2_\mathrm{gr}(x,t) = \epsilon_\mathrm{gr}(x,t) = f\left(f_{1,\mathrm{per}}(x), f_{2,\mathrm{per}}(t)\right)$, where $f_{1,\mathrm{per}}(x)$ and $f_{2,\mathrm{per}}(t)$ are periodic functions of space (in the x direction) and time, respectively. The wavenumber in region 2 (inside the STP grating) is denoted by k'.

The STP grating assumes oblique incidence of the y-polarized electric field in Eq. (12). The x component of the wavevector outside the STP grating, in region 3, reads $k''_{x,mn} = k''_n \sin(\theta''_{mn})$, where $k''_n = k''_0 + n\Omega/v''_\mathrm{r}$ and where $k''_0 = \omega_0/v''_\mathrm{r}$. The corresponding z component of the wavevector in region 3 is calculated using the Helmholtz relation, as $k''_{z,mn} = \sqrt{(k''_{mn})^2 - (k''_{x,mn})^2} = k''_n \cos(\theta''_{mn})$. To determine the spatial and temporal frequencies of the diffracted orders, we consider the momentum conservation law, i.e., $k_{x,\mathrm{diff}} = k''_{x,mn} = k_x + mK$ and the energy conservation law, i.e., $\omega_\mathrm{diff} = \omega_0 + n\Omega$, where $k_{x,\mathrm{diff}}$ and k_x denote the x components of the wavevector of the diffracted and incident fields, respectively, and ω_diff and ω_0 represent the temporal frequencies of the diffracted and incident fields, respectively. Then,

$$\left(k''_0 + n\frac{\Omega}{v''_\mathrm{r}}\right)\sin\left(\theta''_{mn}\right) = k_0\sin(\theta_\mathrm{I}) + mK, \tag{20}$$

where $k_0 = n_1\omega_0/c$. Considering $n_1 = n_3$, the angle of diffraction for the forward ST diffracted orders in region 3 and the backward ST diffracted orders in region 1, i.e., the mth spatial and nth temporal harmonic, yields

$$\sin\left(\theta''_{mn}\right) = \frac{\sin(\theta_\mathrm{I}) + mK/k_0}{1 + n\Omega/\omega_0}, \tag{21}$$

For a given set of incident angles, spatial and temporal frequencies of the grating, and the wavelength of the incident beam, the grating equation may be satisfied for more than one values of m and n. However, there exists a solution only when $|\sin\left(\theta_{mn}\right)| < 1$. Diffraction orders corresponding to m and n satisfying this condition are called *propagating* orders. The other orders yielding $|\sin\left(\theta_{mn}\right)| > 1$ correspond to imaginary z components of the wavevector $k_{z,mn}$ as well as complex angles of diffraction $\sin(\theta_{mn})$. These evanescent orders decrease exponentially with the distance from the grating, and hence, can be detected only at a distance less than a few wavelengths from the grating. The specular order ($m = 0$) is always propagating while the others can be either propagating or evanescent. The modulations with $2\pi/K << \lambda_0$ will produce evanescent orders for $m \neq 0$, while the modulations with $2\pi/K >> \lambda_0$ will yield a large number of propagating orders.

After expanding the field inside the modulated metasurface in terms of the ST diffracted orders (m and n), such ST diffracted orders are phase matched to diffracted orders outside of the metasurface. The electric field inside the metasurface is expressed in terms of a sum of an infinite number of modes, i.e., $\mathbf{E}_2(x,z,t) = \sum_p \mathbf{E}_{2,p}(x,z,t)$, and the corresponding electric field of the pth mode inside the structure may be decomposed into ST Bloch-Floquet plane waves, that is,

$$\mathbf{E}_{2,p}(x,z,t) = \hat{\mathbf{y}}\sum_m\sum_n E'_{pmn}e^{i(k'_{x,pmn}x + k'_{z,pmn}z - \omega_n t)}, \tag{22a}$$

where

$$E'_{pmn} = \frac{(\omega_n/c)^2}{(k'_{x,pmn})^2 + (k'_{z,pmn})^2}\sum_j\sum_q \epsilon_{m-j,n-q}E'_{pjq} \tag{22b}$$

$$k'_{x,pmn} = \left(k'_{p00} + n\frac{\Omega}{v'_\mathrm{r}}\right)\sin\left(\tan^{-1}\left(\frac{k'_{x,p0n}}{k'_{z,p0n}}\right)\right) + mK \tag{22c}$$

and $k'_{z,pmn} = k'_{pmn}\cos(\theta_\mathrm{I})$. Equation (22a) is formed by three summations on modes p, spatial diffractions m, and temporal diffractions n. For ST metasurfaces operating outside the

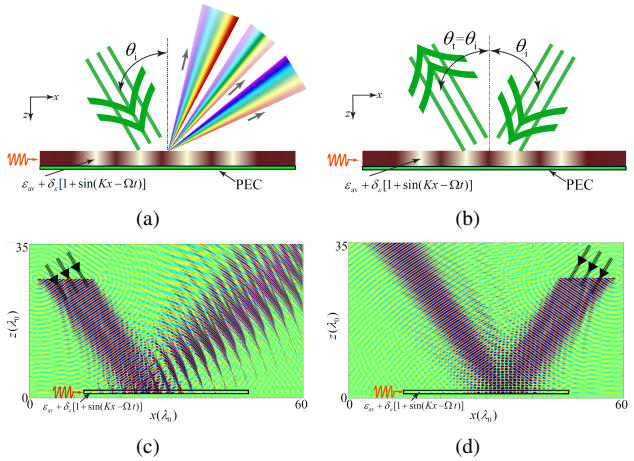

Fig. 11. Nonreciprocal and angle-asymmetric ST diffraction of a reflective STP diffraction grating with a $+x$-traveling STM electric permittivity, i.e., $\epsilon(x,t) = \epsilon_{\text{av}} + \delta_\epsilon[1+\sin(Kx-\Omega t)]$, where $\delta_\epsilon = 0.5$, $\Omega = 0.4\omega_0$, $d = 0.8\lambda_0$. (a) and (d) Forward wave incidence [15]. (b) and (e) Backward wave incidence for nonreciprocal diffraction demonstration [15]. (c) and (f) Backward wave incidence for angle-asymmetric demonstration [15].

diffraction regime only the fundamental spatial order $m = 0$ is scattered which includes an infinite number of temporal harmonics n (where inside the structure each STH is formed by an infinite number of modes p), as in Eq. (13).

The electric field in region 1 reads

$$\mathbf{E}_1 = \hat{\mathbf{y}} E_0 e^{i(k_x x + k_z z - \omega_0 t)} + \hat{\mathbf{y}} \sum_{m,n} E^{\text{R}}_{mn} e^{i(k_{x,mn} x - k_{z,mn} z - \omega_n t)}, \tag{23}$$

where E^{R}_{mn} is the unknown amplitude of the mth reflected ST diffracted orders in region 1, with the wavevectors $k_{x,mn}$ and $k_{z,mn}$. The total electric field in region 3 reads $\mathbf{E}_3 = \hat{\mathbf{y}} \sum_{m,n} E^{\text{T}}_{mn} e^{i(k''_{x,mn} x + k''_{z,mn} z - \omega_n t)}$, where E^{T}_{mn} is the amplitude of the mth transmitted ST diffracted order in region 3, with the wavevectors $k''_{x,mn}$ and $k''_{z,mn}$. To determine the unknown field coefficients of the backward and forward diffracted orders, E^{R}_{mn} and E^{T}_{mn}, we enforce the continuity of the tangential electric and magnetic fields at the boundaries of the grating at $z = 0$ and $z = d$. Thin gratings result in Raman-Nath regime diffraction, where multiple diffracted orders are produced. In contrast, the thick gratings usually result in Bragg regime diffraction, where only one single diffracted order is produced.

Figures 11(a) to 11(d) show the nonreciprocal and angle-asymmetric responses of reflective STP diffraction gratings. Comparing the results of the forward and backward incidence, shown in Figs. 11(c) and 11(d), respectively, one may obviously see that the reflective diffraction by the grating is completely angle-asymmetric. Such an asymmetric reflective diffraction includes asymmetric angles of diffraction and unequal amplitudes of the diffracted orders.

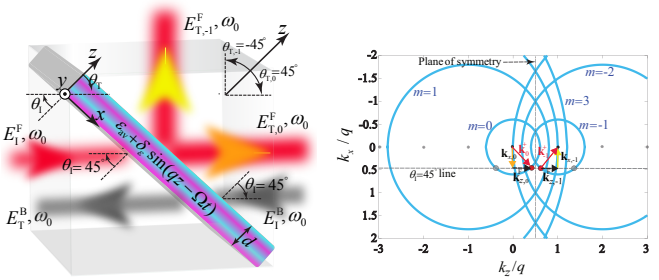

Fig. 12. One-way beam splitting by a STM metasurface. (a) Schematic [11]. (b) Isofrequency diagram at $\omega = \omega_0$ composed of an infinite set of circles centered at $(k_z/q, k_x/q) = (-n, 0)$ with radius $\Gamma(0.5+n)$ [11].

VI. Extraordinary Wave Transformations in ST Metasurfaces

A. Unidirectional Beam Splitter

Beam splitters are quintessential elements in communication systems that are restricted to reciprocal response and suffer from substantial transmission loss. A one-way, tunable and highly efficient beam splitter and amplifier can be realized by taking advantage of coherent electromagnetic transitions through the oblique illumination of ST metasurfaces. Figure 12(a) sketches the nonreciprocal beam transmission and splitting in a STM metasurface. A unidirectional energy and momentum transition occurs from the incident wave-under angle of incidence $\theta_{\text{I}} = 45^\circ$ and temporal frequency ω_0- to the fundamental ($n = 0$) and first lower ($n = -1$) STHs that are transmitted under angles of transmissions $\theta_{\text{T},0} = 45^\circ$ and $\theta_{\text{T},-1} = -45^\circ$, respectively. The two transmitted STHs with 45° angle difference acquire the same temporal frequency as the incident wave, ω_0. We assume the incident electric field in Eq. (12) under the angle of incidence $\theta_{\text{I}} = 45^\circ$ impinges to the periodic STM metasurface.

The structure assumes a sinusoidal ST-varying permittivity with the temporal modulation frequency of $\Omega = 2\omega_0$, and the spatial modulation frequency of $q = 2k_0/\Gamma$. Here, $k_{z,n} = \beta_0 + nq$ and the temporal frequency $\omega_n = (1+2n)\omega_0$, with β_0 being the unknown spatial frequency of the fundamental harmonic. The unknowns of the electric field, that is, A_n and β_0, will be found through satisfying Maxwell's equations. The transmission angle of the mth transmitted STH, $\theta_{\text{T},n}$, satisfies the Helmholtz relation as $k_0^2 \sin^2(\theta_{\text{I}}) + k_n^2 \cos^2(\theta_{\text{T},n}) = k_n^2$, where $k_n = \omega_n / v_{\text{b}}$ denotes the wavenumber of the nth transmitted STH outside the STM metasurface. The angle of transmission $\theta_{\text{T},n}$ reads

$$\theta_{\text{T},n} = \sin^{-1}\left(\frac{k_x}{k_n}\right) = \sin^{-1}\left(\frac{\sin(\theta_{\text{I}})}{1+2n}\right), \tag{24}$$

which demonstrates the spectral decomposition of the transmitted wave. Consequently, the fundamental STH ($n = 0$) and the first lower STH ($n = -1$) with the same temporal frequency ω_0 will be respectively transmitted under the angles of transmission of $\theta_{\text{T},0} = \theta_{\text{I}} = 45^\circ$ and $\theta_{\text{T},-1} = -\theta_{\text{I}} = -45^\circ$ so that they are transmitted under 90° angle difference, presenting the desired beam splitting.

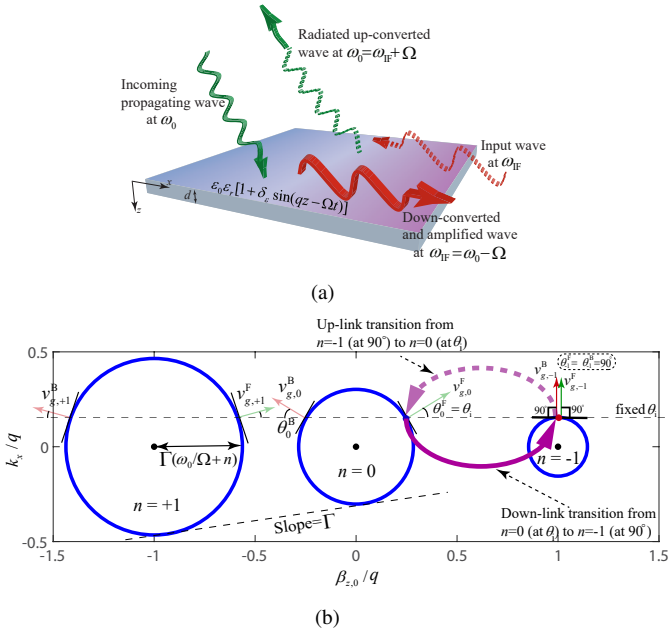

Fig. 13. Antenna-mixer-amplifier metasurface. (a) Schematic representation showing the down-link and up-link wave transformations [56]. (b) Analytical isofrequency dispersion diagram (for $\Gamma = 0.2$ and $\epsilon_m \Longrightarrow 0$) depicting down-link (reception) and up-link (transmission) electromagnetic transitions [56].

Figure 12(b) presents the isofrequency dispersion diagram. This diagram is formed by a $2N+1$ periodic set of double cones (here, only $m=0$ and $n=-1$ harmonics are shown), each of which representing a STH, with apexes at $k_x = 0$, $k_z = -nq$ and $\omega = -2n\omega_0$, and the slope of v_m with respect to $k_z - k_x$ plane. Next, consider oblique incidence of a wave, representing the fundamental harmonic $n=0$ with temporal frequency ω_0, propagating along the $[+x,+z]$ direction. It is characterized by x- and z-components of the spatial frequency, $\mathbf{k}_x = \hat{\mathbf{x}}k_x$ and $\mathbf{k}_z^{\mathrm{F}} = \hat{\mathbf{z}}k_z$. The incident wave shines the medium under the angle of incidence $\theta_I = 45°$ and excites an infinite number of (we truncate it to $2N+1$) STH waves, with different spatial and temporal frequencies of $[k_x, k_{z,n}]$ and ω_n. The first lower STH $n=-1$ acquires identical characteristics as the fundamental ST harmonic, that is, the identical temporal frequency of ω_0 and identical z-component of the spatial frequency of $\mathbf{k}_{z,-1}^{\mathrm{F}} = \mathbf{k}_{z,0}^{\mathrm{F}}$, but opposite x-component of the spatial frequency of $\mathbf{k}_{x,-1} = -\mathbf{k}_{x,0}$. Thus, the $m=-1$ harmonic propagates along the $[-x,+z]$ direction.

B. Antenna-Mixer-Amplifier Functionality

Consider the metasurface in Fig. 13(a), with the thickness of d and a ST periodic electric permittivity. The metasurface in Fig. 13(a) is obliquely illuminated by a y-polarized incident electric field, as shown in Eq. (12). As shown in Fig. 13(a), in the down-link reception state, the space-wave with temporal frequency ω_0 makes a transition to a ST surface wave with temporal frequency $\omega_{IF} = \omega_0 - \Omega$. In the up-link transmission state, the ST surface wave at ω_{IF} makes a transition to a space-wave at $\omega_0 = \omega_{IF} + \Omega$.

Due to the ST periodicity of the metasurface, the spatial and temporal frequencies of the ST harmonics inside the structure read $\gamma_{z,n} = k_z + nq + i\alpha_{z,n}$ and $\omega_n = \omega_0 + n\Omega$, respectively, and the incident angle is $\theta_I = \sin^{-1}(1-\Omega/\omega_0)$. For a strong transition to the $n=-1$ harmonic, the scattered $n=-1$ ST harmonic inside the surface should propagate in parallel to the two ST surface waves along the two boundaries at $z=0$ and $z=d$ ($\theta_{n=-1}=90°$), which gives $\beta_{z,-1}=0$. As a result, the z component of the wave vector inside the medium is purely imaginary, i.e., $\gamma_{z,-1} = i\alpha_{z,-1}$, whereas the incident field wavenumber k_z is purely real.

VII. Conclusion

We presented a comprehensive review of the theory and analysis of wave propagation in space-time (ST) metasurfaces and examples of extraordinary four-dimensional wave transformations in such media. It is shown that ST metasurfaces are capable of four-dimensional electromagnetic wave transformations which are significantly more versatile and useful than the three-dimensional wave transformations of conventional spatially variant static metamaterials and metasurfaces. Recent progress on ST metasurfaces for breaking time-reversal symmetry and reciprocity reveals a great potential for applications of such metasurfaces for low-energy and energy-harvesting telecommunication systems, and compact and integrated non-reciprocal devices, and sub-systems.

References

[1] T. W. Ebbesen, H. J. Lezec, H. Ghaemi, T. Thio, and P. Wolff, "Extraordinary optical transmission through sub-wavelength hole arrays," *Nature*, vol. 391, no. 6668, p. 667, 1998.
[2] S. Taravati and G. V. Eleftheriades, "Programmable nonreciprocal meta-prism," *Sci. Rep.*, vol. 11, no. 1, pp. 1–12, 2021.
[3] G. V. E. Sajjad Taravati, "Full-duplex reflective beamsteering metasurface featuring magnetless nonreciprocal amplification," *Nat. Commun.*, vol. 14, p. 4414, 2021.
[4] S. Taravati and G. V. Eleftheriades, "Microwave space-time-modulated metasurfaces," *ACS Photonics*, 2022.
[5] R. A. Shelby, D. R. Smith, and S. Schultz, "Experimental verification of a negative index of refraction," *Science*, vol. 292, no. 5514, pp. 77–79, 2001.
[6] S. Taravati and G. V. Eleftheriades, "Full-duplex nonreciprocal beam steering by time-modulated phase-gradient metasurfaces," *Phys. Rev. Appl.*, vol. 14, no. 1, p. 014027, 2020.
[7] V. K. Valev, J. Baumberg, B. De Clercq, N. Braz, X. Zheng, E. Osley, S. Vandendriessche, M. Hojeij, C. Blejean, J. Mertens *et al.*, "Nonlinear superchiral meta-surfaces: tuning chirality and disentangling non-reciprocity at the nanoscale," *Adv. Mater.*, vol. 26, no. 24, pp. 4074–4081, 2014.
[8] Y. Hadad, D. L. Sounas, and A. Alù, "Space-time gradient metasurfaces," *Phys. Rev. B*, vol. 92, no. 10, p. 100304, 2015.
[9] S. Taravati, B. A. Khan, S. Gupta, K. Achouri, and C. Caloz, "Nonreciprocal nongyrotropic magnetless metasurface," *IEEE Trans. Antennas Propagat.*, vol. 65, no. 7, pp. 3589–3597, Aug. 2017.
[10] L. Zhang, X. Q. Chen, S. Liu, Q. Zhang, J. Zhao, J. Y. Dai, G. D. Bai, X. Wan, Q. Cheng, G. Castaldi *et al.*, "Space-time-coding digital metasurfaces," *Nat. Commun.*, vol. 9, no. 1, p. 4334, 2018.
[11] S. Taravati and A. A. Kishk, "Dynamic modulation yields one-way beam splitting," *Phys. Rev. B*, vol. 99, no. 7, p. 075101, Jan. 2019.
[12] Z. Wu and A. Grbic, "Serrodyne frequency translation using time-modulated metasurfaces," *IEEE Trans. Antennas Propagat.*, 2019.
[13] S. Taravati and A. A. Kishk, "Advanced wave engineering via obliquely illuminated space-time-modulated slab," *IEEE Trans. Antennas Propagat.*, vol. 67, no. 1, pp. 270–281, 2019.

[14] J. W. Zang, D. Correas-Serrano, J. T. S. Do, X. Liu, A. Alvarez-Melcon, and J. S. Gomez-Diaz, "Nonreciprocal wavefront engineering with time-modulated gradient metasurfaces," *Phys. Rev. Appl.*, vol. 11, no. 5, p. 054054, 2019.

[15] S. Taravati and G. V. Eleftheriades, "Generalized space-time periodic diffraction gratings: Theory and applications," *Phys. Rev. Appl.*, vol. 12, no. 2, p. 024026, 2019.

[16] M. Saikia, K. V. Srivastava, and S. A. Ramakrishna, "Frequency-shifted reflection of electromagnetic waves using a time-modulated active tunable frequency-selective surface," *IEEE Trans. Antennas Propagat.*, vol. 68, no. 4, pp. 2937–2944, 2019.

[17] M. M. Salary, S. Jafar-Zanjani, and H. Mosallaei, "Electrically tunable harmonics in time-modulated metasurfaces for wavefront engineering," *New J. Phys.*, vol. 20, no. 12, p. 123023, 2018.

[18] X. Guo, Y. Ding, Y. Duan, and X. Ni, "Nonreciprocal metasurface with space-time phase modulation," *Light Sci. Appl.*, vol. 8, no. 123, pp. 1–9, 2019.

[19] M. M. Salary, S. Farazi, and H. Mosallaei, "A dynamically modulated all-dielectric metasurface doublet for directional harmonic generation and manipulation in transmission," *Adv. Opt. Mater.*, p. 1900843, 2019.

[20] M. M. Salary and H. Mosallaei, "Time-modulated conducting oxide metasurfaces for adaptive multiple access optical communication," *IEEE Trans. Antennas Propagat.*, vol. 68, no. 3, pp. 1628–1642, 2020.

[21] H. B. Sedeh, M. M. Salary, and H. Mosallaei, "Time-varying optical vortices enabled by time-modulated metasurfaces," *Nanophotonics*, vol. 1, no. ahead-of-print, 2020.

[22] S. Taravati, "Aperiodic space-time modulation for pure frequency mixing," *Phys. Rev. B*, vol. 97, no. 11, p. 115131, 2018.

[23] P. Chu, J. Chen, Z. Xiong, and Z. Yi, "Controllable frequency conversion in the coupled time-modulated cavities with phase delay," *Optics Communications*, vol. 476, p. 126338, 2020.

[24] A. L. Cullen, "A travelling-wave parametric amplifier," *Nature*, vol. 181, p. 332, Feb. 1958.

[25] P. K. Tien, "Parametric amplification and frequency mixing in propagating circuits," *J. Appl. Phys.*, vol. 29, no. 9, pp. 1347–1357, Sept. 1958.

[26] X. Zhu, J. Li, C. Shen, G. Zhang, S. A. Cummer, and L. Li, "Tunable unidirectional compact acoustic amplifier via space-time modulated membranes," *Phys. Rev. B*, vol. 102, no. 2, p. 024309, 2020.

[27] S. Taravati, N. Chamanara, and C. Caloz, "Nonreciprocal electromagnetic scattering from a periodically space-time modulated slab and application to a quasisonic isolator," *Phys. Rev. B*, vol. 96, no. 16, p. 165144, Oct. 2017.

[28] S. Y. Elnaggar and G. N. Milford, "Controlling nonreciprocity using enhanced brillouin scattering," *IEEE Trans. Antennas Propagat.*, vol. 66, no. 7, pp. 3500–3511, 2018.

[29] S. Taravati, "Giant linear nonreciprocity, zero reflection, and zero band gap in equilibrated space-time-varying media," *Phys. Rev. Appl.*, vol. 9, no. 6, p. 064012, Jun. 2018.

[30] K. A. Lurie, D. Onofrei, W. C. Sanguinet, S. L. Weekes, and V. V. Yakovlev, "Energy accumulation in a functionally graded spatial-temporal checkerboard," *IEEE Antennas and Wireless Propagation Letters*, vol. 16, 2017.

[31] S. Taravati, "Application of space-and time-modulated dispersion engineered metamaterials to signal processing and magnetless nonreciprocity," Ph.D. dissertation, École Polytechnique de Montréal, 2017.

[32] H. Barati Sedeh, M. M. Salary, and H. Mosallaei, "Topological space-time photonic transitions in angular-momentum-biased metasurfaces," *Adv. Opt. Mater.*, p. 2000075, 2020.

[33] P. A. Huidobro, E. Galiffi, S. Guenneau, R. V. Craster, and J. Pendry, "Fresnel drag in space–time-modulated metamaterials," *Proc. Natl. Acad. Sci. U.S.A.*, vol. 116, no. 50, pp. 24 943–24 948, 2019.

[34] S. Taravati and G. V. Eleftheriades, "Lightweight low-noise linear isolator integrating phase-and amplitude-engineered temporal loops," *Adv. Mater. Technol*, 2021.

[35] ——, "Pure and linear frequency-conversion temporal metasurface," *Phys. Rev. Appl.*, vol. 15, no. 6, p. 064011, 2021.

[36] S. Taravati and C. Caloz, "Mixer-duplexer-antenna leaky-wave system based on periodic space-time modulation," *IEEE Trans. Antennas Propagat.*, vol. 65, no. 2, pp. 442 – 452, Feb. 2017.

[37] A. Alvarez-Melcon, X. Wu, J. Zang, X. Liu, and J. S. Gomez-Diaz, "Coupling matrix representation of nonreciprocal filters based on time-modulated resonators," *IEEE Trans. Microw. Theory Techn.*, vol. 67, no. 12, pp. 4751–4763, 2019.

[38] X. Wu, X. Liu, M. D. Hickle, D. Peroulis, J. S. Gómez-Díaz, and A. Á. Melcón, "Isolating bandpass filters using time-modulated resonators," *IEEE Trans. Microw. Theory Techn.*, vol. 67, no. 6, pp. 2331–2345, 2019.

[39] L. Zhang, Z. X. Wang, R. W. Shao, J. L. Shen, X. Q. Chen, X. Wan, Q. Cheng, and T. J. Cui, "Dynamically realizing arbitrary multi-bit programmable phases using a 2-bit time-domain coding metasurface," *IEEE Trans. Antennas Propagat.*, vol. 68, no. 4, pp. 2984–2992, 2019.

[40] V. Bacot, M. Labousse, A. Eddi, M. Fink, and E. Fort, "Time reversal and holography with spacetime transformations," *Nat. Phys.*, vol. 12, no. 10, p. 972, 2016.

[41] S. A. Stewart, T. J. Smy, and S. Gupta, "Finite-difference time-domain modeling of space–time-modulated metasurfaces," *IEEE Trans. Antennas Propagat.*, vol. 66, no. 1, pp. 281–292, 2017.

[42] S. Inampudi, M. M. Salary, S. Jafar-Zanjani, and H. Mosallaei, "Rigorous space-time coupled-wave analysis for patterned surfaces with temporal permittivity modulation," *Opt. Mater. Express*, vol. 9, no. 1, pp. 162–182, 2019.

[43] S. Y. Elnaggar and G. N. Milford, "Generalized space-time periodic circuits for arbitrary structures," *arXiv preprint arXiv:1901.08698*, 2019.

[44] N. Wang, Z.-Q. Zhang, and C. Chan, "Photonic floquet media with a complex time-periodic permittivity," *Phys. Rev. B*, vol. 98, no. 8, p. 085142, 2018.

[45] S. Taravati and A. A. Kishk, "Space-time modulation: Principles and applications," *IEEE Microw. Mag.*, vol. 21, no. 4, pp. 30–56, 2020.

[46] G. A. Ptitcyn, M. S. Mirmoosa, and S. A. Tretyakov, "Time-modulated meta-atoms," *Phys. Rev. Res.*, vol. 1, no. 2, p. 023014, 2019.

[47] Z.-X. Du, A. Li, X. Y. Zhang, and D. F. Sievenpiper, "A simulation technique for radiation properties of time-varying media based on frequency-domain solvers," *IEEE Access*, vol. 7, pp. 112 375–112 383, 2019.

[48] A. Li, Y. Li, J. Long, E. Forati, Z. Du, and D. Sievenpiper, "Time-moduated nonreciprocal metasurface absorber for surface waves," *Optics Letters*, vol. 45, no. 5, pp. 1212–1215, 2020.

[49] J. L. Wentz, "A nonreciprocal electrooptic device," *Proc. IEEE*, vol. 54, no. 1, pp. 97–98, 1966.

[50] S. Taravati, "Self-biased broadband magnet-free linear isolator based on one-way space-time coherency," *Phys. Rev. B*, vol. 96, no. 23, p. 235150, Dec. 2017.

[51] M. Oudich, Y. Deng, M. Tao, and Y. Jing, "Space-time phononic crystals with anomalous topological edge states," *Phys. Rev. Res.*, vol. 1, no. 3, p. 033069, 2019.

[52] M. Chegnizadeh, M. Memarian, and K. Mehrany, "Non-reciprocity using quadrature-phase time-varying slab resonators," *J. Opt. Soc. Am. B*, vol. 37, no. 1, pp. 88–97, 2020.

[53] S. Taravati and A. A. Kishk, "Space-time-varying surface-wave antenna," in *2018 18th International Symposium on Antenna Technology and Applied Electromagnetics (ANTEM)*. IEEE, 2018.

[54] J. Zang, X. Wang, A. Alvarez-Melcon, and J. S. Gomez-Diaz, "Nonreciprocal yagi–uda filtering antennas," *IEEE Antennas Wirel. Propagat. Lett.*, vol. 18, no. 12, pp. 2661–2665, 2019.

[55] M. Liu, A. B. Kozyrev, and I. V. Shadrivov, "Time-varying metasurfaces for broadband spectral camouflage," *Phys. Rev. Appl.*, vol. 12, no. 5, p. 054052, 2019.

[56] S. Taravati and G. V. Eleftheriades, "Space-time medium functions as a perfect antenna-mixer-amplifier transceiver," *Phys. Rev. Appl.*, 2020.

[57] Z. Manzoor and S. Taravati, "Enhanced resolution imaging by aperiodically perturbed photonic time crystals," in *2020 Conference on Lasers and Electro-Optics (CLEO)*. IEEE, 2020, pp. 1–2.

[58] J. Li, C. Shen, X. Zhu, Y. Xie, and S. A. Cummer, "Nonreciprocal sound propagation in space-time modulated media," *Phys. Rev. B*, vol. 99, no. 14, p. 144311, 2019.

[59] M. Liu, D. A. Powell, Y. Zarate, and I. V. Shadrivov, "Huygens' metadevices for parametric waves," vol. 8, no. 3, p. 031077, 2018.

[60] S. Y. Elnaggar and G. N. Milford, "Modelling space-time periodic structures with arbitrary unit cells using time periodic circuit theory," *arXiv preprint arXiv:1901.08698*, 2019.

[61] S. Taravati and G. V. Eleftheriades, "Mixer-antenna medium," in *2019 13th International Congress on Artificial Materials for Novel Wave Phenomena (Metamaterials)*. IEEE, 2019.

[62] F. Biancalana, A. Amann, A. V. Uskov, and E. P. O'reilly, "Dynamics of light propagation in spatiotemporal dielectric structures," *Phys. Rev. E*, vol. 75, no. 4, p. 046607, 2007.

[63] F. R. Morgenthaler, "Velocity modulation of electromagnetic waves," *IEEE Trans. Microw. Theory Tech.*, vol. 6, no. 2, pp. 167–172, 1958.

[64] R. Fante, "Transmission of electromagnetic waves into time-varying media," *IEEE Trans. Antennas Propagat.*, vol. 19, no. 3, pp. 417–424, 1971.